Water Vapor Barrier Properties of Transparent SnO_2-SiO_x Composite Films on Polymer Substrate

Won Hoe Koo, Soon Moon Jeong, Sang Hun Choi, and Hong Koo Baik*

Department of Metallurgical Engineering, Yonsei University, Seoul 120-749, Korea

Sung Man Lee

Department of Advanced Material Science and Engineering, Kangwon National University, ChunCheon, Kangwon-do 200-701, Korea

Se Jong Lee

Department of Materials Engineering, Kyunbcgsung University, Busan 608-736, Korea

Received: June 2, 2004; In Final Form: October 1, 2004

Composite thin films consisting of silicon oxide and tin oxide have been deposited on polycarbonate substrates as gas barrier films, using a thermal evaporation process in an oxygen gas environment. Water vapor permeation through the composite films is significantly affected by the chemical interaction of water vapor with the composite oxide films and the microstructure of the composite oxide films. The chemical interaction of water vapor with oxide films has been investigated by the considering the refractive index obtained from ellipsometry and the OH group peak from X-ray photoelectron spectroscopy, and the microstructure of the composite oxide films has been characterized using atomic force microscopy. As the tin oxide is added to the silicon oxide, the refractive index and OH group peak intensity of the composite films increase, and the water vapor transmission rate through the composite oxide films shows a lower value than that through the single-element oxide films, such as tin oxide and silicon oxide alone. The results are discussed in terms of the chemical interaction with water vapor and the microstructure of the oxide films. Finally, the water permeation mechanism related to the diffusivity and solubility of water vapor was qualitatively analyzed on the basis of the results of Fourier transform infrared spectroscopy.

1. Introduction

Inorganic transparent oxide films such as silicon and aluminum oxide on polymer substrates have been widely used as a gas barrier in the fields of food packaging, medical devices, and recently, flexible display industries. Especially for passivation of organic light-emitting devices (OLEDs) requiring extremely low oxygen and water vapor transmission rates, relatively dense oxynitride films such as AlO_xN_y and SiO_xN_y, compared to AlO_x and SiO_x, have been studied as gas barrier materials using sputtering and plasma-enhanced chemical vapor deposition (PECVD) methods.[1−3] However, because sputtering methods including electron beam evaporation cause severe radiation damage to the underlying organic layer in OLEDs due to the energetic beams such as ions and X-rays and the electron beam produced during deposition, and because PECVD additionally requires the use of toxic gas and high deposition temperature, these deposition methods are undesirable for depositing the passivation layer of OLEDs.[4−8] Although thermal evaporation is a desirable deposition method because it avoids radiation damage, there have been no studies on the gas barrier properties of films deposited by thermal evaporation besides the SiO_x films, because little oxide materials can be thermally evaporated and the films deposited by thermal evaporation have an open microstructure due to their low adatom mobility. Because water vapor interacts with oxides[9] and thus the water transmission rate can be affected by the chemistry of oxides, it is important to consider the chemical interaction with water vapor when depositing oxide materials.

In this paper, we report the water barrier properties of thermally evaporated composite oxide films consisting of tin oxides and silicon oxides. The fact that these composite films showed a better water barrier performance than the SiO_x and SnO_2 films is discussed in terms of the chemical interaction with water vapor and the microstructure of the oxide films.

2. Experiment

The composite films were deposited by thermal evaporation on optical grade polycarbonates (PC), glass, and Si(100) wafer substrates in an atmosphere of oxygen. The PC substrates with the thickness of 200 μm, provided by i-components Co., Ltd., have no "antiblock" particle-inducing microscale defects in the deposited films and have a very smooth surface of rms (surface roughness) below 1 nm. Before the deposition, the glass and Si substrates were cleaned sequentially by trichloroethylene, acetone, and alcohol. An anti-electrostatic gun was used to remove the surface electrostatic charge on the PC substrates following the cleaning with alcohol. The base pressure of 6.7×10^{-4} Pa was achieved using a turbomolecular pump, and the working pressure was kept at 1.1×10^{-2} Pa with the flow rate of oxygen of 2 sccm. The evaporation source materials were mixed oxides of SiO and SnO_2 with various atomic concentration ratios. The powders of SiO and SnO_2 with purity of 99.99% and 99.9%, respectively, were mixed according to atomic

10.1021/jp047617d CCC: $27.50
Published on Web 11/13/2004

concentration ratios from 5:1 to 1:2 and were evaporated on the tungsten boats. The film growth rate was maintained at 0.1 nm/s by using a quartz crystal monitor, and the film thickness was fixed at 80 nm. To ensure the same thickness for each composition, tooling factors were calibrated with an α-step surface profiler.

The optical transmittance and reflectance of the thin films deposited on glass substrates were recorded in the wavelength ranges of 250−800 nm by using a spectrophotometer (Shimadzu UV-3101PC). An Al-coated reflector was used as a reference for the reflectance. The refractive index for the thin films deposited on the Si(100) substrates was measured at 633 nm by an L117 ellipsometer (Gaertner Scientific Corp.). The structure of the composite films on the PC substrates was determined by XRD (Rigaku, D/max-RINT 2700) operating at 30 kV, 20 mA, using a Cu $K\alpha_1$ line ($\lambda = 0.154056$ nm), and all the films showed amorphous structure. The surface morphology of the films on the PC substrates was examined by atomic force microscopy (AFM) with a Digital Instruments Nanoscope II. The AFM images of 1×1 μm^2 were obtained in tapping mode at a scan rate of 1 Hz, using Si tips with a tip radius of ~10 nm. The chemical compositions and the chemical bonding states of the composite films with different atomic concentrations of SiO and SnO_2 were analyzed by monochromatic X-ray photoelectron spectroscopy (XPS) (VG Scientific, ESCARLAB 220-IXL) using an Al Kα X-ray with energy 1486.6 eV and a takeoff angle of 90°. Narrow-scan spectra of all regions of interest were recorded with 20 eV pass energy, and the binding energy scale was referred to the C1s peak of the carbon contaminating the sample surface at a value of 284.6 eV. The water vapor transmission rate (WVTR) and activation energy for water vapor permeation were measured at 100% relative humidity (RH) using a Permatran W 3/31 (Modern Controls, Inc.). The samples were masked with aluminum foil having a 5 cm^2 gas exposure area for water vapor transmission, and the data were taken at temperatures ranging from 27.8 to 47.8 °C. The water absorption properties of films deposited on the Si substrates were analyzed with a FTIR spectrometer (Perkin-Elmer Spectrum GX) after storage of the samples in a 100% RH and 50 °C environment for 24 h. The reflectance spectra were collected at 8 cm^{-1} resolution by adding 256 scans. Since the WVTR arrives at the steady state within 24 h, storage in a 100% RH and 50 °C environment for 24 h provides enough time for the water absorption of the deposited films to reach the steady state.

3. Results and Discussion

3.1. Chemical Composition and Optical Properties. The composition and chemical states of the deposited composite films were analyzed by XPS. The deposited composite films from the evaporation source in which SiO_2 and SnO_2 were mixed with atomic concentration ratios of 5:1, 3:1, 2:1, and 1:2 had SnO_2 atomic percents of 5, 24, 45, and 80, respectively. From the Si2p and Sn3d peak deconvolution, we found that the deposited composite films were composed of SiO_x films and SnO_x films with oxygen compositions of around 1.7 and 2, respectively.

Variations of the refractive index of SnO_2-SiO_x composite films with SnO_2 content are presented in Figure 1a. The films of 80% SnO_2 show the maximum refractive index, which is consistent with the results of Feldman et al. for ZrO_2-SiO_2 and $Y_2O_3-SiO_2$ and of Koo et al. for CeO_2-SiO_2 composite films fabricated by coevaporation.[10−12] The SnO_2 films exhibit the lower refractive index, rather than the films with 80% SnO_2,

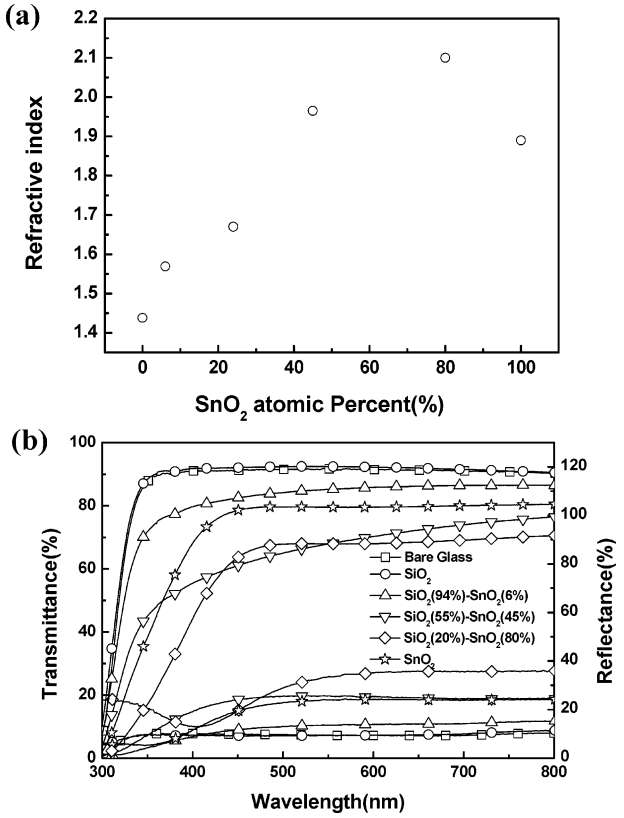

Figure 1. (a) Variations in the refractive index of composite films deposited by thermal evaporation and (b) the specular transmittance and reflectance spectra of composite films with varying SnO_2 atomic concentration (0%, 6%, 45%, 80%, 100%).

implying a lower packing density. Because the refractive index of the films was closely related to the microstructure and the packing density, Feldman et al. remarked that the unusual variations in the refractive index originated from the densification of composite films.

Figure 1b presents the transmittance and reflectance spectra of composite films with regard to different compositions. As the SnO_2 content increases, the optical absorption of composite films occurs at longer wavelengths. This occurs because SnO_2 begins to absorb at a wavelength of around 450 nm. Respectively, the transmittance and reflectance of the deposited films decrease and increase with the SnO_2 content. However, composite films over a composition of around 45% SnO_2 show lower transmittance and higher reflectance than pure SnO_2 films. The 80% SnO_2 films show the lowest transmittance and highest reflectance. This tendency is associated with the variations of the refractive index of the composite films. Since all the films were deposited on silica glass substrate of refractive index 1.52, the reflectance of the composite films exhibits the maximum value at the composition of the highest refractive index, and thus the transmittance shows the minimum value at the same composition.

3.2. Water Vapor Transmission Rate (WVTR) and Activation Energy. Figure 2a shows the water vapor transmission rate measured at 37.8 °C through the composite films deposited on the PC substrate. The pure SiO_x and SnO_x films provide approximately 2.4 times improvement in WVTR, compared to the bare PC substrate (34 $g/m^2 \cdot day$). The poor water vapor barrier properties of the SiO_x films are compared to about 15 times improvement in WVTR of the SiO_x films on poly(ethylene terephthalate) (PET) produced by PECVD[13] and attributed to the loose microstructure due to the low adatom mobility of

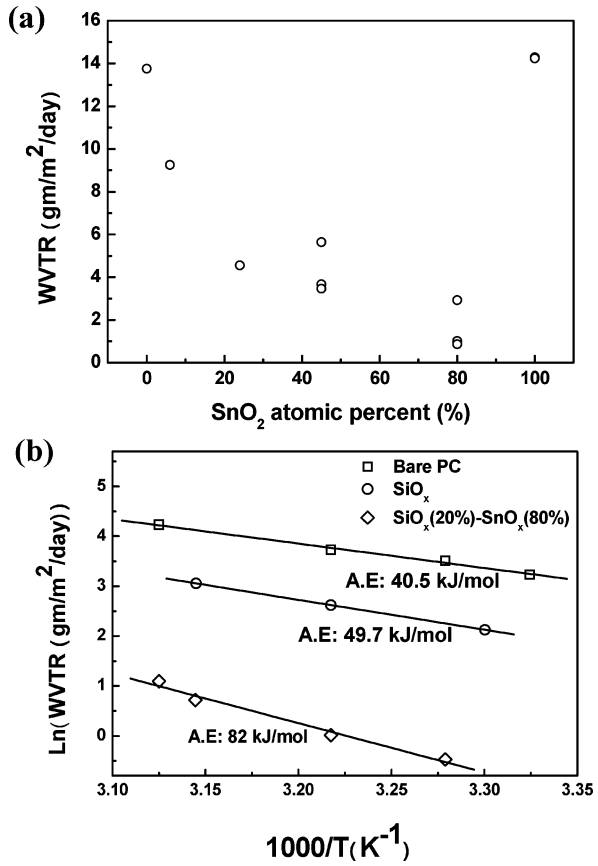

Figure 2. (a) Water vapor transmission rate (WVTR) for the composite films on PC at 37.8 °C as a function of the atomic concentration of tin oxide and (b) dependence of water vapor transmission rate on reciprocal temperature through the bare PC (□), PC/SiO_x films (○), and PC/80% SnO_2 films (◇).

thermal evaporation. However, as the SnO_x content in the composite films increases, the WVTR decreases, reaching the lowest value of about 1 g/m^2·day at a composition of 80% SnO_x. The deposition of the composite films with 80% SnO_x on the PC substrate shows a reduction of about 34 times in the water vapor transmission rate, which suggest that the 80% SnO_x films have more effective water vapor barrier properties than the SiO_x, AlO_x, and AlO_xN_y films deposited by PECVD, electron beam evaporation, and sputtering methods.[2,13,14]

The temperature dependence of water vapor transport through the coated polymers below their glass transition temperature can be described by the following Arrhenius equation:

$$\Pi = \Pi_o \exp(-\Delta E/RT)$$

where Π is the transmission rate, ΔE is the activation energy of permeation, R is the universal gas constant, T is absolute temperature, and Π_o is a constant unique to the system. Figure 2b shows the water vapor transmission data measured between 27.8 and 47.8 °C, presented in Arrhenius form with the activation energy calculated from its slope. The activation energy for water vapor permeation through the thermally evaporated SiO_x barrier film is about 9 kJ/mol higher than that measured for the bare PC (40.5 kcal/mol), and the composite film of 80% SnO_2 has a considerably higher activation energy of 82 kcal/mol for water vapor permeation, which is similar to the activation energy value for water vapor transmission of AlO_xN_y/PET deposited by magnetron sputtering.[3] It has been known that water molecules with large dipole moments interact chemically with the oxide films, and then additional energy is required to induce water vapor to be adsorbed on the voids or pores of SiO_x films for further permeation.[15] Therefore, the higher activation energy in SiO_x films and 80% SnO_2 films is due to the chemical interaction of water vapor with the oxide films during the water vapor permeation, but the degree of the chemical interaction is dependent on the chemistry as well as the porosity of the deposited materials.

Considering the low kinetic energy of the evaporated species in thermal evaporation, the enhanced water vapor barrier performance and significantly increased activation energy for water vapor permeation in the composite films are closely associated with the intrinsic properties of the composite materials according to mixing of SiO_x and SnO_x rather than the films' densification due to the high adatom mobility in sputtering. We have investigated the the physical and chemical aspects of the influence of the composite films on water vapor permeation.

3.3. Chemical Effects. Water has a large dipole moment and lone-pair electrons, and thus is a good donor. Molecular adsorption occurs by acid/base interaction between water vapor and the oxides. Therefore, strong adsorption on the internal surface of pores and on the top surface of oxide films occurs easily in more basic oxides with the generation of the OH group on the surface.[9] Since the basicity of oxides, defined as the average electron donor power, is closely related to the oxides' polarizability, which can be expressed as the refractive index, oxides with a higher polarizability and refractive index result in higher OH group density on the top surface and on the internal surface within pores because of a stronger interaction with water vapor.[16,17] The OH groups formed within pores may interact with permeating water vapor, interrupt the continuous permeation of water vapor, and thus decrease the water vapor transmission rate. The bond strength between OH groups and water bonded to the OH groups is so strong that desorption of water vapor bonded to OH groups begins to occur above 150 °C,[18,19] and thus the additional energy is needed for the water vapor permeation through the oxide films with the surface OH groups within pores. In general, the substitution of oxygen by nitrogen in oxides increases the polarizability and refractive index, as observed in TiO_xN_y, AlO_xN_y, and SiO_xN_y.[20−22] Erlat et al. reported that AlO_xN_y films deposited on PET have a lower water vapor transmission rate and higher activation energy than AlO_x films because of the stronger interaction of water vapor with the AlO_xN_y films.[3]

Figure 3 shows the deconvoluted O1s XPS peaks of the deposited films with SnO_2 content of 0, 24, 80, and 100%. The O1s peak of the SnO_2 films in Figure 3d shows the peak related to the OH groups at around 531.6 eV with the O1s peak of fwhm 1.33 eV, corresponding to the Sn^{4+}, at around 530.3 eV. In contrast, the O1s peak of the SiO_x films shows no peaks related to the OH groups in Figure 3a, except for the O1s peak with fwhm 1.63 eV for SiO_x. Because the polarizability and refractive index of SnO_2 are higher than those of SiO_x, a higher OH group density is formed on the surface and confirmed by the XPS results of Figure 3. As the SnO_2 concentration increases, the portion of the O1s peak corresponding to OH groups increases, and the composite films with 80% SnO_2 show a higher OH group density than the pure SnO_2 films, which is a result of the higher polarizability and refractive index of 80% SnO_2 films, as shown in Figure 1a.

The OH groups due to the interaction of water vapor with oxides can be generated on the internal surface of pores, which is a pathway of water vapor permeation through the oxide films, in addition to the top surface. Therefore, the continuous transfer of water vapor is restricted by the interaction between the formed

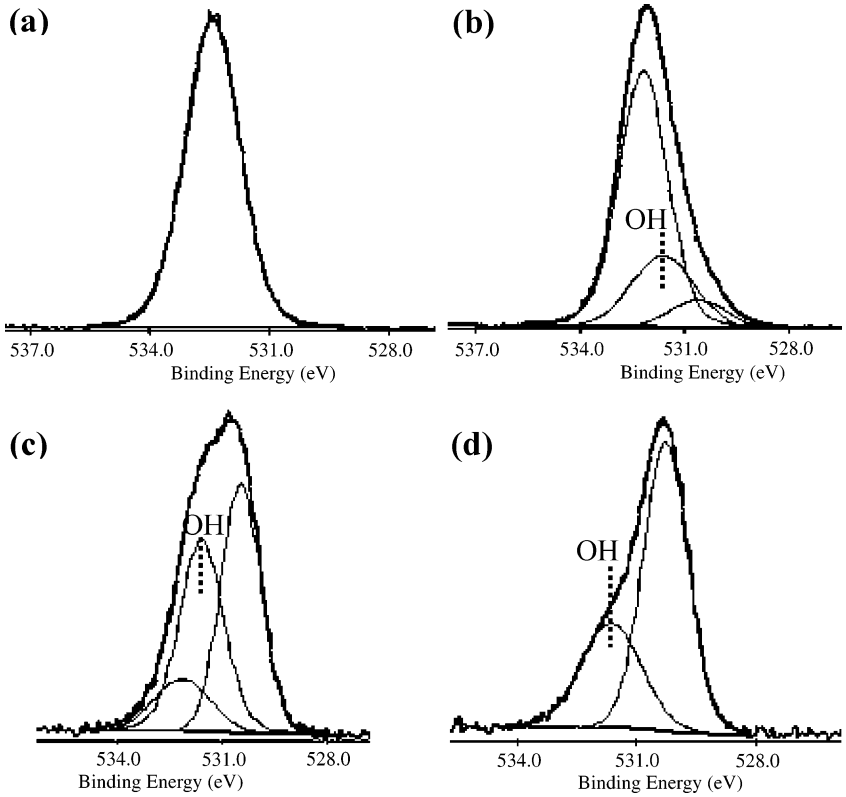

Figure 3. Deconvoluted O1s XPS peaks of the deposited films with the SnO_2 content of (a) 0, (b) 24, (c) 80, and (d) 100%.

OH groups and water vapor, and thus the 80% SnO_2 films with the highest OH group density show the lowest water vapor transmission rate and a greatly increased activation energy for water vapor permeation, as seen in Figure 2. However, although the SnO_2 films have a high refractive index of about 1.9, the water vapor transmission rate is similar to that of the SiO_x films with a refractive index of about 1.44. Here we should consider the influence of the film porosity on the water vapor permeation, because if the pore size and density are too large and high, the permeating water vapor would be expected to penetrate the films with little interaction through the central pore space away from the surface OH groups within pores. The physical effect related to the packing density and the microstructure of the composite films on water vapor barrier properties will be discussed below.

3.4. Physical Effects. Generally, the thin films deposited with low adatom mobility at room temperature have an open structure consisting of spherical grains and pores between grains, and the pores act as significant paths for water vapor permeation. The packing density, representing the porosity of thin films, is closely related to the relative refractive index value of the deposited thin films for the bulk value. The packing density can be simply calculated using the following equation:

$$n_f = pn_s + (1 - p)n_v$$

where p, n_f, n_s, and n_v are the packing density, the index of the film, the index of the solid part of film (that is, grains or columns), and the index of pores in the film, respectively. By applying the refractive indexes 1.52 of a bulk silica glass and 2.2 of a bulk SnO_2 for n_s and $n_v = 1$ for air, we obtained the packing densities of 85% and 74% for the SiO_x films and the SnO_2 films, respectively. Figure 4 shows the AFM images of the SiO_x films, the 80% SnO_2 films, and the SnO_2 films coated on the PC substrate. All of them consist of small spherical grains, and among them the SiO_x films and the SnO_2 films show larger spherical grains than the 80% SnO_2 films. Generally, as the pore size between grains increases with the grain size in a low adatom mobility process like thermal evaporation, the SiO_x films and the SnO_2 films with larger grain size show a lower packing density with the larger pore size and thus a high water vapor transmission rate. Especially the SnO_2 films, despite their high polarizability, show a high water vapor transmission rate due to this loose microstructure. However, the addition of about 20% SiO_x results in the densification of the deposited composite films, as observed in the refractive index of Figure 1a and small grain size of Figure 4b. When the pore size of the composite films with high refractive index is small enough to induce the interaction between the permeating water vapor and the OH groups formed on the internal surface within the pores, the water vapor transmission rate for the composite films can decrease and the activation energy for water vapor permeation can increase. Therefore, the 80% SnO_2 films show a low water vapor transmission rate and high activation energy due to their high refractive index and densely packed microstructure, whereas the SnO_2 films show the high water vapor transmission rate due to the loose microstructure, despite their high refractive index.

3.5. Water Permeation Mechanism. The permeability of the deposited films is a product of the diffusivity and solubility of water vapor on the deposited films. Since the thickness of the deposited films is constant, the permeability of the deposited films for water vapor is the same as the water vapor transmission rate at steady state, and by comparing the relative solubilities of water vapor for the deposited films at steady state, we can qualitatively evaluate the influence of the diffusivity and solubility on the water permeation properties of the deposited films. We measured the relative solubilities of water vapor for the deposited films by FT-IR. Figure 5 represents the FT-IR reflectance spectra ranging from 3000 to 3800 cm^{-1} related to the water absorption for the composite films after storage at 100% RH and 50 °C for 24 h. Since 24 h is enough time for the system to reach the steady state, the water absorption of the

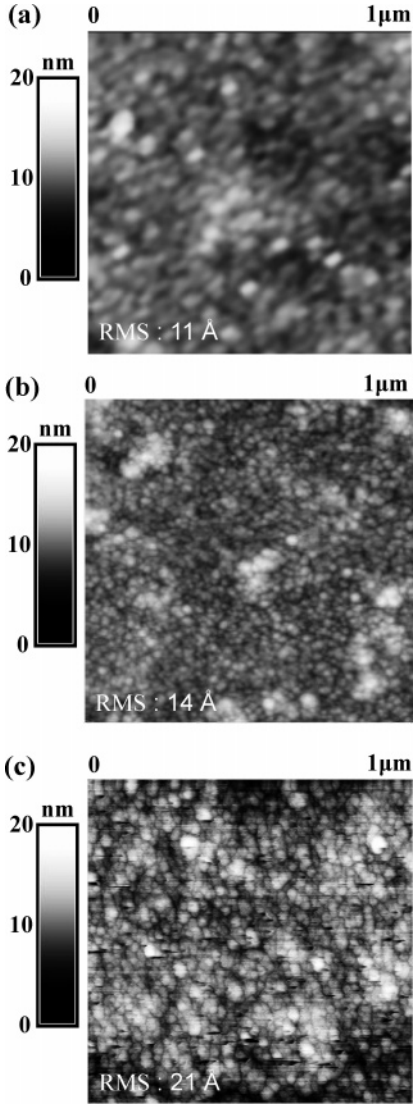

Figure 4. AFM images of (a) the SiO_x films, (b) the 80% SnO_2 films, and (c) the SnO_2 films coated on the PC substrate, taken in tapping mode.

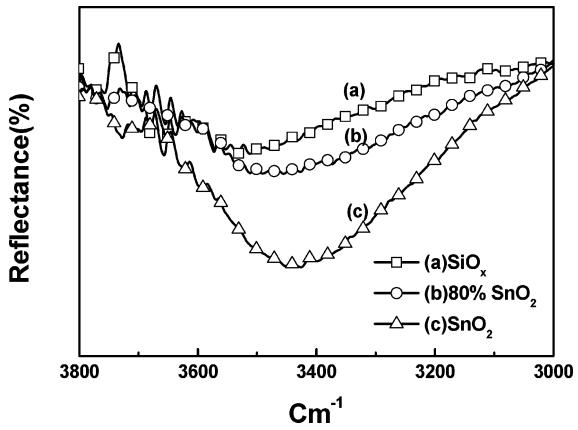

Figure 5. FT-IR reflectance spectra ranging from 3000 to 3800 cm^{-1} related to the water absorption for the SiO_x, 80% SnO_2, and SnO_2 films.

deposited films in Figure 5 can be considered the relative water solubility of the deposited films. The SiO_x films with low polarizability in Figure 5a show much lower water solubility than the SnO_2 films with high polarizability in Figure 5c. Because the WVTR of the SiO_x films is similar to that of the SnO_2 films despite the large difference in water solubility, we can predict that the diffusivity of the SiO_x films and the SnO_2 films with the loose microstructure dominantly contributes to the WVTR. We preclude the possibility that the diffusivity of the SnO_2 films is much lower than that of the SiO_x films because the SnO_2 films have the lower packing density. The 80% SnO_2 films show higher water solubility than the SiO_x films but much lower water solubility than the SnO_2 films. These results, observed by FT-IR, are in contrast to those observed by XPS, in which the 80% SnO_2 films showed the highest OH group density. Since FT-IR provides information for the entire thickness of the films while XPS provides information for only about 50 Å from the top surface, FT-IR results are closely associated with the microstructure of the deposited films. Although the 80% SnO_2 films with the higher refractive index show the higher OH group density on the surface in XPS than the SnO_2 films, the 80% SnO_2 films show much lower water solubility in FT-IR than the SnO_2 films. This is because the 80% SnO_2 films have the denser microstructure and high packing density. By comparison of the water solubility and the WVTR between the 80% SnO_2 films and the SiO_x films, we can conclude that the low WVTR of the 80% SnO_2 films is predominantly attributed to the low diffusivity, and thus the 80% SnO_2 films present a high activation energy of 84 kcal/mol for the transport of water vapor due to their strong interaction with water vapor and their densely packed microstructure.

4. Conclusion

The water barrier properties of composite films consisting of silicon oxide and tin oxide, deposited by thermal evaporation on polycarbonate substrates, have been studied. Water vapor permeation through the composite films is significantly affected by the chemical interaction of water vapor with the composite oxide films and the microstructure of the composite oxide films. As the tin oxide is added to the silicon oxide, the refractive index and OH group peak intensity of the composite oxide films increase due to the increased polarizability, and the composite films have more densely packed microstructure with decreasing grain size. Therefore, the 80% SnO_2 films show the lowest water vapor transmission rate and highest activation energy for water vapor permeation with the lowest diffusivity, compared to the pure SiO_x and SnO_2 films, because of the increased interaction of water vapor with the densely packed composite oxide films.

Acknowledgment. S.M.L. thanks the KISTEP for financial support through the research program of the national research laboratory.

References and Notes

(1) Vogt, M.; Hauptmann, R. *Surf. Coat. Technol.* **1995**, *74*−*75*, 676.

(2) Erlat, A. G.; Henry, B. M.; Ingram, J. J.; Mountain, D. B.; McGuigan, A.; Howson, R. P.; Grovenor, C. R. M.; Briggs, G. A. D.; Tsukahara, Y. *Thin Solid Films* **2001**, *388*, 78.

(3) Erlat, A. G.; Henry, B. M.; Ingram, J. J.; Grovenor, C. R. M.; Briggs, G. A. D.; Chater, R. J.; Tsukahara, Y. *J. Phys. Chem. B* **2004**, *108*, 883.

(4) Bulovic, V.; Tian, P.; Burrows, P. E.; Gokhale, M. R.; Forrest, S. R.; Thompson, M. E. A. *Appl. Phys. Lett.* **1997**, *70*, 2954.

(5) Han, S.; Feng, X.; Lu, Z. H.; Johnson, D.; Wood, R. *Appl. Phys. Lett.* **2003**, *82*, 715.

(6) Hung, L. S.; Tang, C. W.; Manson, M. G.; Raychaudhuri, P.; Madathil, J. *Appl. Phys. Lett.* **2001**, *74*, 544

(7) Hung, L. S.; Liao, L. S.; Lee, C. S.; Lee, S. T. *Appl. Phys. Lett.* **1999**, *86*, 4607.

(8) Cambell, S. A. *The Science and Engineering of Microelectronic Fabrication*; Oxford University Press: New York, 1996.

(9) Henrich, V. E.; Cox, P. A. *The Surface Science of Metal Oxides*; Cambridge University Press: New York, 1996.

(10) Feldman, A.; Farabaugh, E. N.; Haller W. K.; Sanders D. M.; Stempniak R. A. *J. Vac. Sci. Technol. A* **1986**, *4*, 2969.
(11) Feldman, A.; Ying, X.; Farabaugh, E. N. *Appl. Opt.* **1989**, *28*, 5229.
(12) Koo, W. H.; Jeong, S. M.; Choi, S. H.; Baik, H. K.; Lee, S. J.; Song, K. M. *Thin Solid Films* **2004**, *468*, 28.
(13) Tropsha, Y. G.; Harvey, N. G. *J. Phys. Chem. B* **1997**, *101*, 2259.
(14) Deng, C. S.; Assender, H. E.; Dinelli, F.; Kolosov, O. V.; Briggs, G. A. D.; Miyamoto, T.; Tsukahara, Y. *J. Polym. Sci. Part B: Polym. Phys.* **2000**, *38*, 3151.
(15) Erlat, A. G.; Spontak, R. J.; Clarke, R. P.; Robinson, T. C.; Haaland, P. D.; Tropsha, Y.; Harvey, N. G.; Vogler, E. A. *J. Phys. Chem. B* **1999**, *103*, 6074.
(16) Dimitrov, V.; Komatsu, T. *J. Solid State Chem.* **2003**, *163*, 100.
(17) Takeda, S.; Fukawa, M.; Hayashi, Y.; Matsumoto, K. *Thin Solid Films* **1999**, *339*, 220.
(18) Feng, A.; McCoy, J.; Munir, Z. A.; Cagliostro, D E. *J. Colloid Interface Sci.* **1996**, *180*, 276.
(19) Yamazoe, N.; Fuchigami, J.; Kishikawa, M. *Surf. Sci.* **1979**, *86*, 335.
(20) Mohamed, S. H.; Kappertz, O.; Ngaruiya, J. M.; Niemeier, T.; Drese, R.; Detemple, R.; Wakkad, M. M.; Wuttig, *M. Phys. Stat. Sol.* **2004**, *201*, 90.
(21) Dreer, S.; Krismer, R.; Wilhartitz, P.; Friedbacher, G. *Thin Solid Films* **1999**, *354*, 43.
(22) Mohite, K. C.; Khollam, Y. B.; Mandale, A. B.; Patil, K. R.; Takwale, M. G. *Mater. Lett.* **2003**, *57*, 4170.